

Standard, Random and Optimum Array Conversions from Two-pole Resistance Data

Dale F. Rucker¹ and Danney R. Glaser^{2,*}

¹hydroGEOPHYSICS, Inc., 2302 N. Forbes Blvd., Tucson, AZ 85745

Email: drucker@hgiworld.com; druck8240@gmail.com

²Washington River Protection Solutions, LLC, 2440 Stevens Center Place, MSIN H6-13, Richland, WA 99354

*Now at Hager GeoScience, Inc., 596 Main St., Woburn, MA 01801

Email: danneyglaser@gmail.com

ABSTRACT

We present an array evaluation of standard and non-standard arrays over a hydrogeological target. We develop the arrays by linearly combining data from the pole-pole (or 2-pole) array. The first test shows that reconstructed resistances for the standard Schlumberger and dipole-dipole arrays are equivalent or superior to the measured arrays in terms of noise, especially at large geometric factors. The inverse models for the standard arrays also confirm what others have presented in terms of target resolvability, namely the dipole-dipole array has the highest resolution. In the second test, we reconstruct random electrode combinations from the 2-pole data segregated into inner, outer, and overlapping dipoles. The resistance data and inverse models from these randomized arrays show those with inner dipoles to be superior in terms of noise and resolution, and that overlapping dipoles can cause model instability and low resolution. Finally, we use the 2-pole data to create an optimized array that maximizes the model resolution matrix for a given electrode geometry. The optimized array produces the highest resolution and target detail. Thus, the tests demonstrate that high quality data and high model resolution can be achieved by acquiring field data from the pole-pole array.

Introduction

There are many examples in the geophysical literature of electrical resistivity array evaluation to determine the best means to image the subsurface. One of the most comprehensive was that performed by Dahlin and Zhou (2004), where ten standard arrays were compared in a series of tests using synthetic geological models. Each array had different strengths in terms of resolution, acquisition efficiency, depth of signal penetration, and signal-to-noise (S/N). Other examples of array evaluation for both field and synthetically derived models included Dey *et al.* (1975), Saydam and Duckworth (1978), Batayneh (2001), Candansayar and Basokur (2001), and Seaton and Burbey (2002). Most of the studies concluded that the dipole-dipole array has very high resolution and low S/N, whereas the Wenner and Schlumberger arrays have a slightly lower resolution, but better signal penetration and noise characteristics. The pole-pole array also has high S/N, but is one of the lowest resolving arrays.

One means of increasing the utility of the resistivity method is to combine two or more arrays

together, which may take advantage of particular features of individual arrays, such as high resolution and high S/N. For example, Kaufmann and Quinif (2001) and Zhou *et al.* (2002) combined Wenner, Schlumberger, and dipole-dipole arrays to map sink-holes. Again, Dahlin and Zhou (2004) noted that the imaging quality of some mixed arrays is similar to the better resolved individual image and that the data from the lower resolution array provides little to no improvement. Alternatively, Leontarakis and Apostolopoulos (2012) used image stacking by calculating the geometric mean of resistivity from a number of arrays to produce a final model that appeared to be less prone to artifacts compared to individual and mixed arrays. In all of these multiple dataset and multiple model approaches, a significant amount of field and processing time is necessary to capture each of the different arrays.

Two separate tracks of investigation into the resistivity method have almost rendered issues of resolution, acquisition efficiency, and S/N obsolete. Firstly, Niwas and Israil (1989), Xu and Noel (1993), and Lehmann (1995) described a means of selecting a base set of four-pole electrodes from which other

four-pole electrode pairs can be calculated using superposition. Thus, by making a relatively small number of strategic measurements, other desired arrays can simply be calculated and there would be little need to acquire multiple arrays for testing. Blome *et al.* (2011) showed the same type of conversion for a base three-pole (*i.e.*, pole-dipole) dataset to calculate other three-pole combinations. In each case, the noise from the base 3- or 4-pole combination is additive and Blome's approach would appear to be highly advantageous given that only two combinations are necessary to calculate any other combination. Up to six 4-pole combinations are required to cover the complete 4-pole dataset. Rucker (2012) demonstrated a 2-pole to 4-pole conversion for long electrode data, where four calculations are always needed for any 4-pole combination.

The second track of investigation includes calculating the optimal array based on maximizing the subsurface resolution as defined by the inverse model resolution matrix. Stummer *et al.* (2004) introduced the concept of deriving an optimal array configuration that is computationally efficient and combines standard and non-standard electrode combinations. Since then, a number of researchers have expanded the methodology by which to search for and practically use the optimal configuration, including Wilkinson *et al.* (2006), Loke *et al.* (2010), Al Hagrey (2012), Wilkinson *et al.* (2012), and Loke *et al.* (2014). The resolution from the optimal arrays is far superior to any standard array (*e.g.*, pole-pole, dipole-dipole, pole-dipole, Schlumberger, or Wenner). In this work, we combine the two tracks of investigation to calculate the optimal 4-pole array from a measured 2-pole dataset. We first compare the acquired pole-pole data, converted to the standard dipole-dipole and Schlumberger arrays, to the measured standard arrays over the same target. The comparison is to demonstrate the difference in measured and calculated potentials and resulting target definition and resolution from inverse models of each array. We then demonstrate the results from other 4-pole conversions, including a randomized (as demonstrated in Rucker, 2012) and optimal set. The results will demonstrate that superior arrays for acquisition and modeling can be obtained with little effort.

Site Description

Electrical resistivity data for multiple arrays were acquired over a series of infiltration galleries. The galleries, or trenches as they are known, were designed to dispose liquid radiological waste associated with plutonium production at the Hanford site in the mid-1950s (Gephart and Lundgren, 1995). The series of eight trenches, located to the west of the BX tank farm

(Fig. 1), received 15×10^6 L of sodium nitrate waste between 1954 and 1955 (Lindenmeier *et al.*, 2002). Several steel cased wells were installed for geophysical well logging to detect neutron and spectral gamma emitting contaminants. In general, the spectral gamma logging revealed high Cs-137 concentrations in the top 10 m of soil, and in some cases Co-60 to depths of 14 m (Rucker *et al.*, 2013). A soil characterization borehole also revealed significant nitrate concentrations from depths 17 to 61 m below ground surface. The sodium nitrate was the target for electrical resistivity investigation.

Sediments throughout the Hanford site are glacial-fluvial as a result of great floods that swept through the Columbia Basin during the past 15,000 years. The major formations from bottom to top include a Pliocene-age Ringold formation consisting of overbank deposits from the ancestral Columbia River, a Pliocene-age calcified paleosol Cold Creek unit, and a Pleistocene-age Hanford formation resulting from the catastrophic flood deposits of glacial Lake Missoula (Gee *et al.*, 2007). The Hanford formation can be further divided into subunits based on loose boundaries of coarse and fine grained fractions. Electrically, these sediments are relatively resistive compared to the sodium nitrate waste target.

Array Optimization

The definition of optimal electrode configurations can be considered from a combination of important factors such as signal strength, depth of penetration, the ability to complete acquisition in a short period of time, and the resolving capability of the configuration. Much of the work into developing optimized arrays has been focused on the last item, where electrode pairs are chosen such that the model resolution of the subsurface is maximized. For example, Maurer *et al.* (2000) demonstrated with a Schlumberger sounding example that a subset of measurements contribute significantly to resolving the geological features of the subsurface while other measurements contribute very little. Diagonal elements of the model resolution matrix, \mathbf{R} , indicated the relative importance of individual data points. The model resolution matrix is defined by $\mathbf{m}^{\text{fit}} = \mathbf{R}\mathbf{m}^{\text{true}}$ (Menke, 1984), where \mathbf{m}^{fit} is the estimate of the model resistivities determined by the inversion process, and \mathbf{m}^{true} comprises the unknown true resistivities (Wilkinson *et al.*, 2006). If each model cell is perfectly resolved then \mathbf{R} is the identity matrix. Later, Stummer *et al.* (2004) generalized the work of Maurer *et al.* (2000) by searching for the best subset of configurations that maximizes the model resolution by starting with a base dipole-dipole array and adding only those configurations that increase the model resolution. The added configurations were chosen from a comprehensive list and new

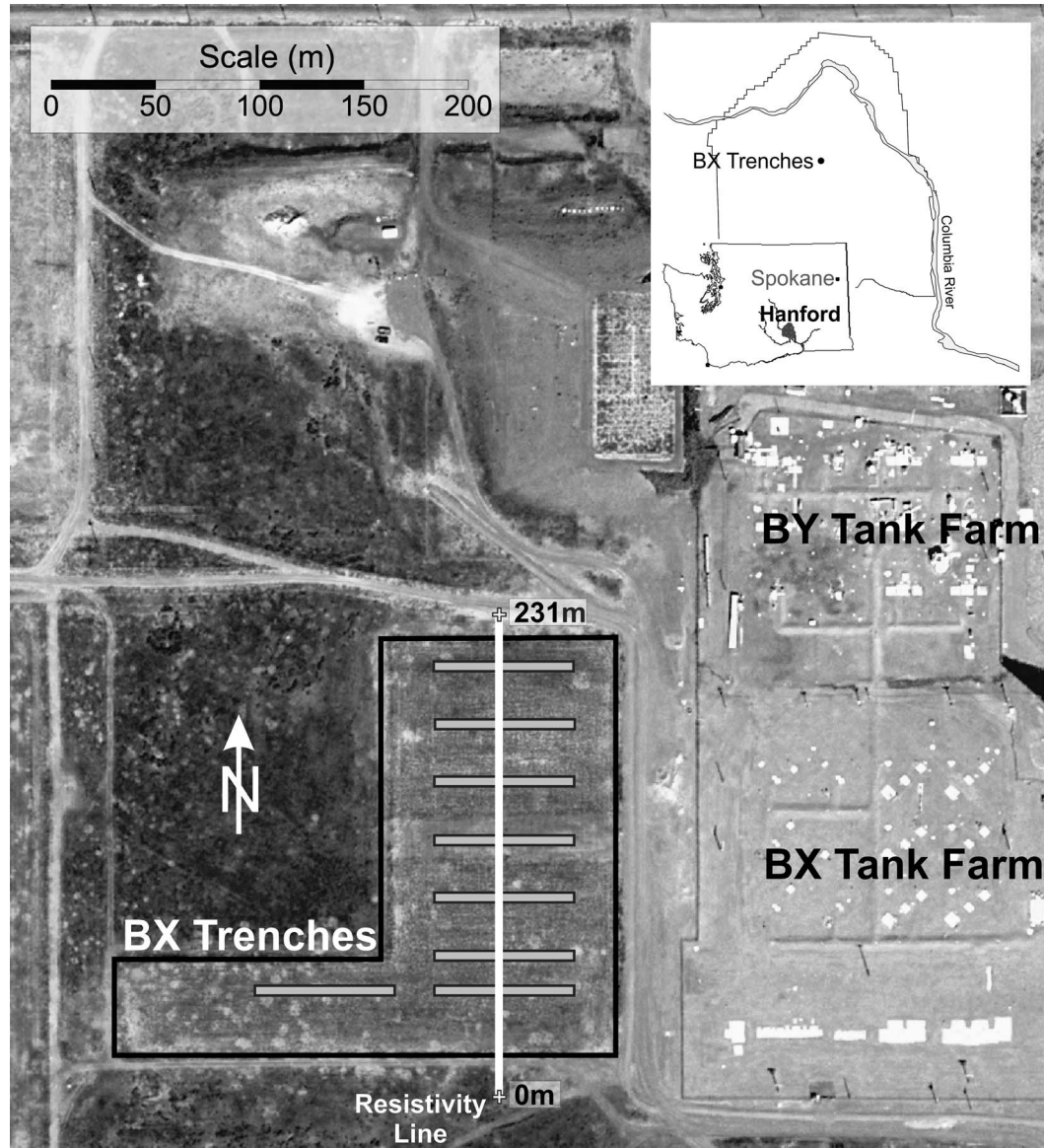


Figure 1. Location of the Hanford site and resistivity study in central Washington.

configurations were tested incrementally using a goodness function (GF) to determine the effect on the resolution. Their work showed that non-standard electrode configurations could be chosen that greatly enhances the ability of the resistivity method to resolve important areas of the subsurface.

Over the last decade, effort in determining the optimal array has focused on the computational difficulty of searching for the subset of electrode configurations that provide the greatest resolution. Wilkinson *et al.* (2006) compared three strategies for finding the optimal set and determined that the Compare R method is more accurate, but computationally slower than the original or Modified GF search.

Based on its performance, Loke *et al.* (2010a, b) developed new algorithms for the Compare R method and used new computational hardware (the Graphical Processing Unit, or GPU) to speed the search for electrode subsets.

In our work, we use the Compare R method for searching the best subset of electrode pairs to increase resolution of the subsurface. Operationally, the Compare R methodology starts with a base set of electrode combinations. The high resolution of the dipole-dipole array makes it a good starting point, and the Compare R algorithm uses configurations of a unit electrode spacing for dipole length (*i.e.*, *a*-spacing) and dipole separations (*n*-spacing) from

1 to 6. With 78 electrodes used in our study, the base dipole-dipole set for the optimal array included 435 combinations. To this base set, new combinations were added incrementally. To reduce the number of possible combinations in which to explore, those exhibiting extremely large geometric factors and other less stable configurations such as overlapping dipoles were excluded. The examples presented below, using overlapping dipoles generated from randomized combinations, confirmed the instability observed in other's work (e.g., Stummer *et al.*, 2004; Wilkinson *et al.*, 2006). Additionally, electrode combinations that were not symmetrical about the survey line were made symmetrical by adding the complement to the other side of the line.

The resolution updating procedure was conducted iteratively by adding a small number of combinations with each trial. In this case, we added 5% to the number of electrode combinations with each iteration. The model resolution matrix was then updated and compared to the previous iteration. Those combinations that increased the resolution were kept; those combinations that worsened the resolution were discarded. The procedure was terminated when the number of optimal combinations reached 8,000.

Methodology

The following section describes arrays acquired and calculated from transfer resistance data for conventional arrays, random arrays, and the optimized array based on the Compare R method (Loke *et al.*, 2010).

Conventional Arrays

The survey line for the array conversion demonstration was placed perpendicular to the series of BX trenches (Fig. 1). The line was 231 m with 78 electrodes spaced every 3 m. The resistivity data were acquired with a SuperSting R8 (by AGI, Austin, Texas). The complete dataset with all measured arrays included the Schlumberger array with 1,482 measurements, dipole-dipole array with 580 measurements, and pole-pole array with 3,003 measurements. The remote poles were placed 800 m and 1,200 m away for the transmitting and receiving dipoles, respectively. No reciprocal measurements were taken. However, the SuperSting R8 output file contains a repeat voltage measurement error based on two measurements taken consecutively. The final voltage is recorded as the average of both measurements and the error is calculated as the difference between the measurements divided by the averaged resistance, which is then recorded as a percentage.

A comparison of the raw resistance data is shown in Fig. 2. The data are plotted as a pseudo-plot with

distances along the line taken as an average between the transmitter and receiver electrode positions for pole-pole and dipole-dipole, and as the average of the internal receiver electrodes for the Schlumberger array. The data are shown to segregate naturally by their a-spacing value, which is the (di)pole distance for pole-pole and dipole-dipole arrays or the distance between transmitter electrodes for the Schlumberger array. The signal strength for the pole-pole array is shown to be significantly higher than the dipole-dipole and Schlumberger arrays. A minimum resistance value of 0.25 ohms was obtained for the pole-pole array relative to 0.0053 ohms for the dipole-dipole array and 0.0012 ohms for the Schlumberger array. Unexpectedly, the minimum resistance values for the Schlumberger array are lower than those of the dipole-dipole array. However, the average resistance for the Schlumberger array is 30% higher than the resistance for the dipole-dipole array.

The reconstructed 4-pole resistance from measured 2-pole resistance data is calculated by (Rucker, 2012):

$$U_{ABMN} = U_{AM} - U_{AN} - U_{BM} + U_{BN}, \quad (1)$$

where subscripts A and B refer to the transmission electrode pair and M, N refer to the receiving electrode pair needed for the completion of the resistance (U) measurement. For the error (or noise) of each data pair, the following relationship is used:

$$E_{ABMN} = E_{AM} + E_{AN} + E_{BM} + E_{BN}. \quad (2)$$

Equation (1) was used to calculate the equivalent Schlumberger and dipole-dipole arrays from measured pole-pole data, and the results of the calculation can be observed in Fig. 2 in direct comparison to the measured data. The pseudo-plots of each calculated array are shown to align well with the measured data, and the scatterplot of measured vs. calculated show very little deviation from a near perfect fit. The measured data from Schlumberger and dipole-dipole arrays are shown to have some noise, but the calculated values for those particular pairs appear to be less noisy because of the higher quality pole-pole data.

The resistance data from the three arrays were inverted individually to build a representation of subsurface resistivity. There are many published articles on electrical resistivity inversion to which the reader may refer (e.g., Loke *et al.* (2013) and the references therein). To keep the analysis simple, only the measured data were modeled. Given the goodness of fit for the calculated versus measured data, the inverse models for the calculated data would not have shown much difference relative to the models of the measured data. RES2DINVx64 was used for the inversion and the three datasets converged to a root mean square (RMS) error

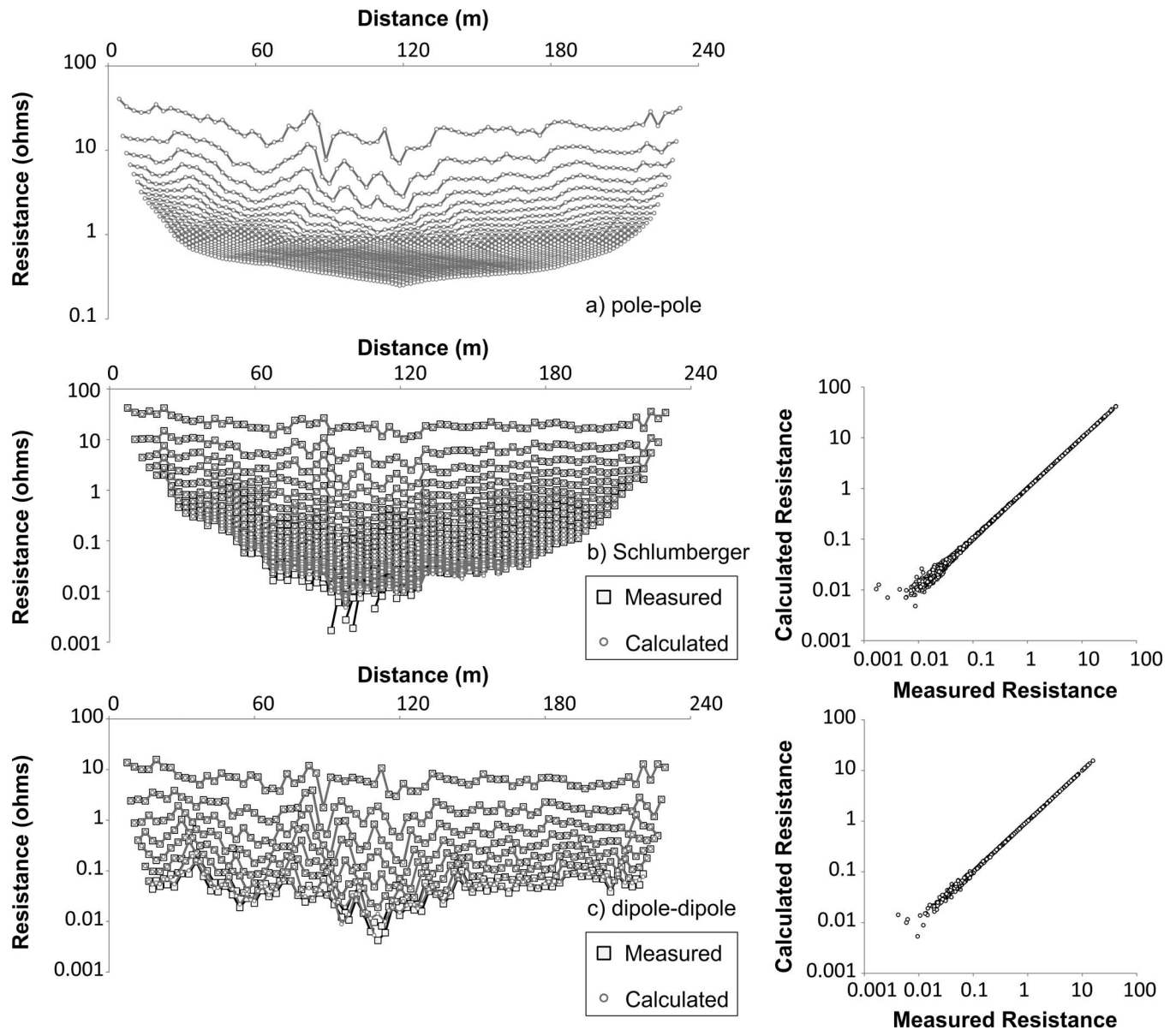


Figure 2. Pseudo-plot of data acquired with a) pole-pole array, b) Schlumberger array, and c) dipole-dipole array. For the Schlumberger and dipole-dipole array, both measured and calculated resistances are compared as a pseudo-plot and scatter plot.

less than 5% within four iterations. The pole-pole array converged with an RMS of less than 1.5% in four iterations, thus providing a qualitative noise comparison among the three arrays.

Figures 3 and 4 show the results of the inverse modeling. In Fig. 3, contours of the logarithmically-transformed resistivity show similar features among the three arrays. There is a large low resistivity target between a distance of 80 and 100 m, which is likely the direct result of nitrate-laden waste disposed in the series of BX trenches. Other near-surface resistive features can also be traced within all three models, for example at

distances of 80 and 180 m. Major differences between the arrays can be seen in the depth of investigation, where the pole-pole images are significantly deeper than the other two arrays, and in the shape and amplitude of the low resistivity target. For ease of plotting, the pole-pole array has been truncated to a depth of 50 m, but the entire model extended to a depth of 162 m.

Figure 4 shows the model resolution of each array. \mathbf{R} may be viewed as a filter that blurs the true values of the subsurface resistivities (Stummer *et al.*, 2004). To ensure a fair comparison of \mathbf{R} between the arrays of our test, the model discretization and all model constraints

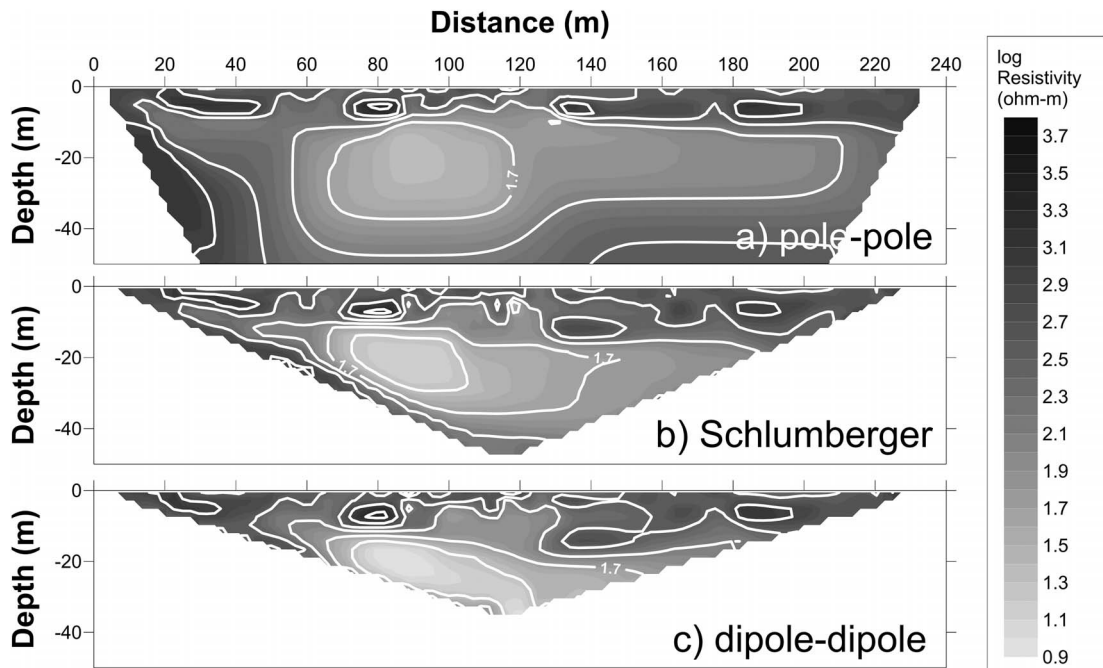


Figure 3. Inverse model results using measured data for a) pole-pole, b) Schlumberger, and c) dipole-dipole arrays.

were kept constant. Inverse model grid discretization included a 3-m width in the horizontal direction and variable layering from 1.1 to 8.5 m. Constraints included using the L2 norm, initial model dampening factor of 0.15, and increasing the dampening by a factor of 1.1 with depth. When evaluating results, Fig. 4 shows that

the model resolution is highest for the dipole-dipole array and the lowest for the pole-pole array. For example, the average depth for the 0.063 isopleth (or log value of -1.2) is 6.8 m, 7.7 m, and 8.2 m for pole-pole, Schlumberger, and dipole-dipole arrays, respectively. Table 1 lists several other statistics for the models

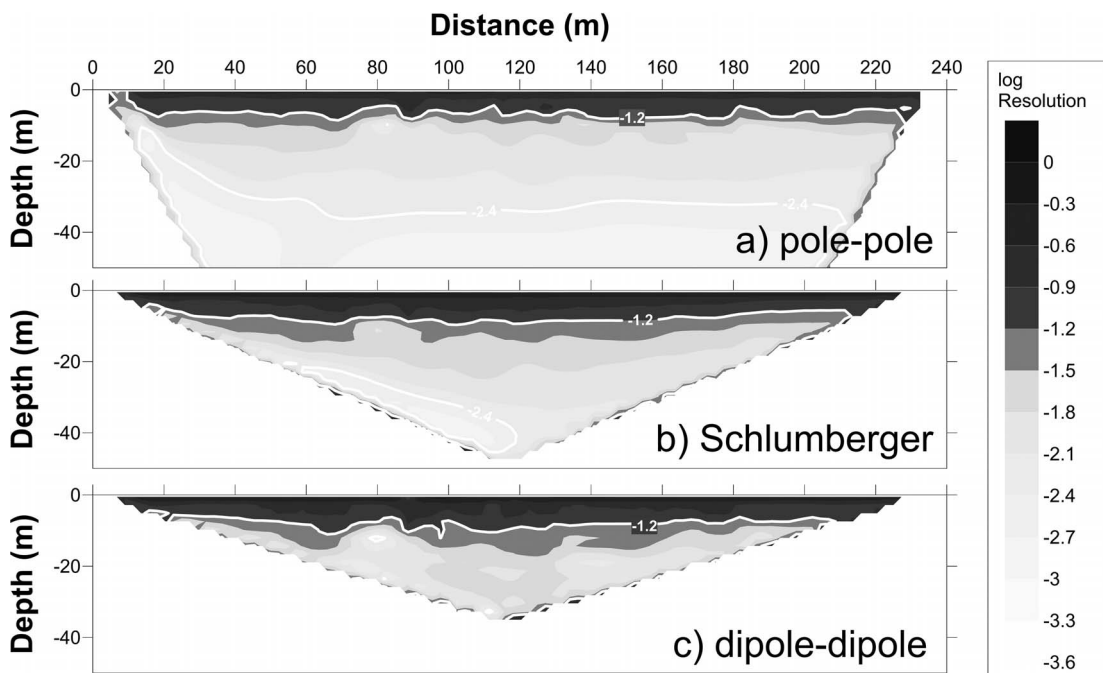


Figure 4. Model resolution for a) pole-pole, b) Schlumberger, and c) dipole-dipole arrays.

Table 1. Resistivity and resolution statistics from inversion models.

Array	Resistivity range (ohm-m)	Avg. resolution	Avg. depth for resolution isopleth = 0.063 (m)
Pole-pole	22.2 to 2,787	0.042	6.8
Schlumberger	13.9 to 3,007	0.096	7.7
Dipole-dipole	8.5 to 2,674	0.111	8.2
Random with inner dipoles	11.4 to 5,380	0.120	8.8
Random with outer dipoles	6.6 to 5,859	0.117	9.1
Random with overlapping dipoles	19.6 to 8,563	0.098	8.7
Random with all dipoles	12.8 to 6,220	0.107	9.1
Optimum	8.5 to 5,038	0.140	11.2

to allow for direct comparison between them. Of the three standard arrays tested, the dipole-dipole has the highest average resolution of 0.111.

Random Arrays

The next test was to create a random set of 4-pole data from the 2-pole data. The algorithm for the randomized array first created a unique list comprising four integers that incorporated the 78 electrodes. A lookup function then combed the 2-pole dataset for the combinations associated with the random list and calculated the resistances according to Eq. (1). In addition, the geometric factor (K) was calculated as:

$$K = 2\pi \left(\left| \frac{1}{AM} \right| - \left| \frac{1}{AN} \right| - \left| \frac{1}{BM} \right| + \left| \frac{1}{BN} \right| \right)^{-1}, (3)$$

where distances between electrodes A, B, M, and N were used in the formulation. According to Xu and Noel (1993) and Rucker *et al.* (2011), we would expect the total number of 4-pole combinations from a 78-electrode dataset to be in excess of 4.2×10^6 . In this example, we chose to limit our random set to 5×10^4 combinations and positive geometric factors less than 1×10^6 m. Furthermore, the random combinations were divided into inner dipoles, outer dipoles, and overlapping dipoles. Carpenter and Habberjam (1956) referred to these combinations as Alpha, Beta, and Gamma arrangements, respectively. The Wenner and Schlumberger arrays would be considered inner dipole arrangements and the dipole-dipole would be considered an outer dipole arrangement. Overlapping dipoles are constructed from transmitting electrode pairs straddling or interleaving the receiving electrodes. Figure 5 shows the distribution of these random data as resistance versus K. The data are shown to align along a fairly narrow band of apparent resistivity values, especially the inner dipole set of Fig. 5(a). The data from outer dipoles (Fig. 5(b)) span a much broader range of geometric factors, and the data

from overlapping dipoles (Fig. 5(c)) show fairly noisy resistance values at smaller K.

The individual and combined random dipole models were created using a subset of 4,100 and 5,400 resistance records, extracted from each dipole dataset, respectively. The dataset for each model was based on those measurements with the lowest calculated noise according to Eq. (2). Using superposition, the repeat errors for each 2-pole combination, as provided from the instrument data file, were added and an error value less than 1.5% was used as the cut-off in developing the final model input file. Each dataset was inverted using similar parameters and discretized grid as the standard arrays. The only exception was choosing to invert apparent resistivity and not logarithm of apparent

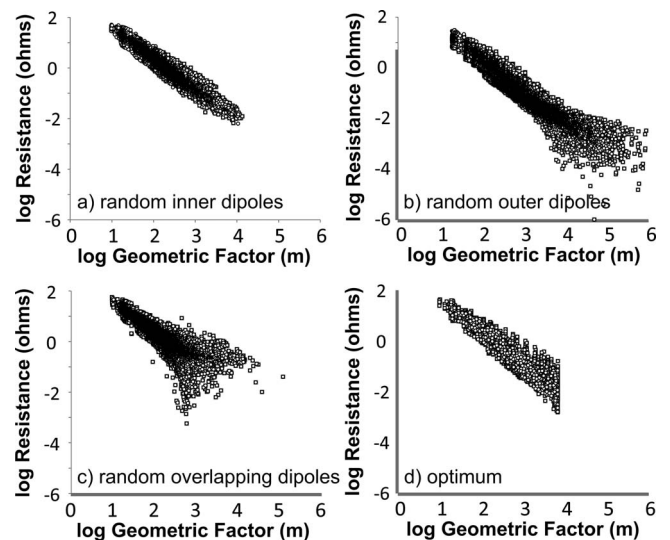


Figure 5. Resistance versus geometric factor for random and optimum 4-pole combinations calculated from the 2-pole dataset. The random data are segregated by inner, outer, and overlapping dipoles.

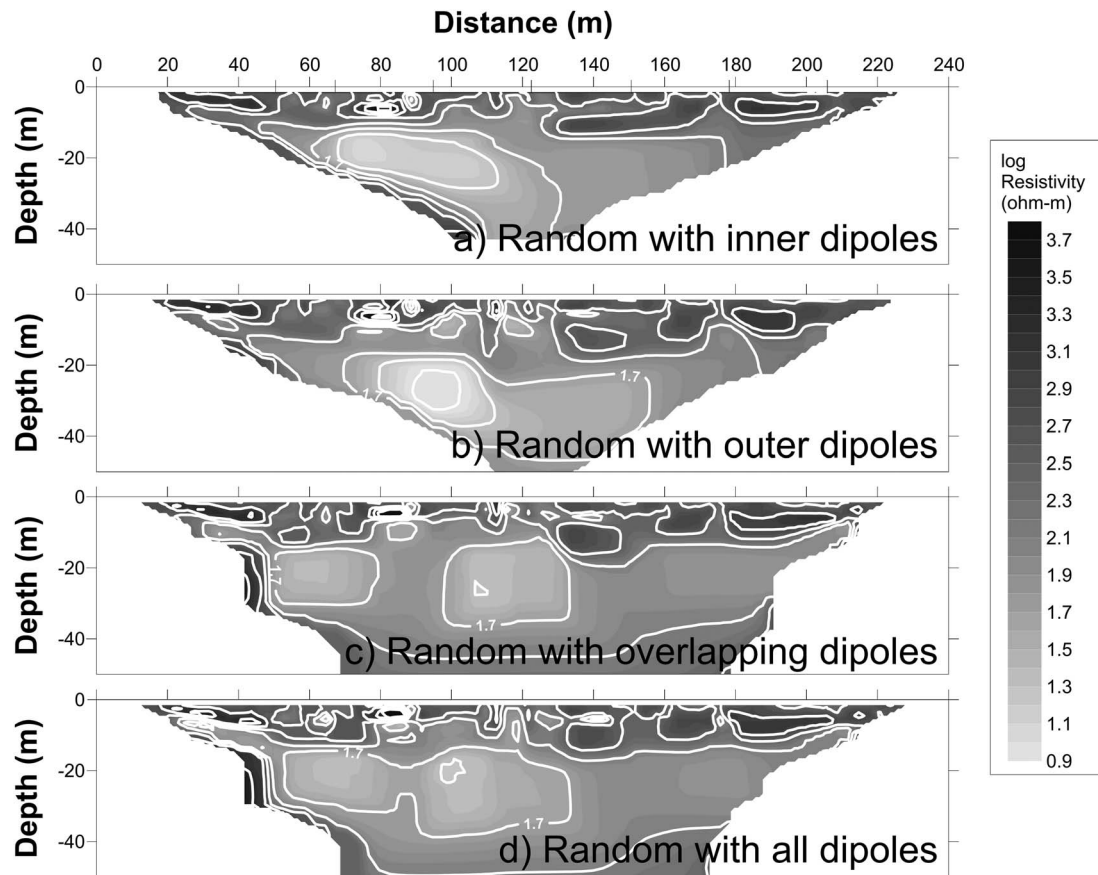


Figure 6. Inverse model results using randomly generated dipoles, segregated by a) inner dipoles, b) outer dipoles, c) overlapping dipoles, and d) all dipoles.

resistivity for the two examples that included overlapping dipole data because negative apparent resistivities being calculated in the code cannot be log transformed. The negative apparent resistivity was likely a result of the differences in the way the geometric factor is calculated, which could have become negative in the inversion code. Each random array converged to an RMS value less than 5% within four iterations.

The contours of resistivity in the random dipole models (Fig. 6) show a similar low resistivity target among all models and with those of Fig. 3. The models of overlapping dipoles, whether alone (Fig. 6(c)) or together with other dipoles (Fig. 6(d)), show a dampened target from the choice of how the apparent resistivity data were used. However, the overlapping dipoles show a deeper investigation depth. The resolution contours of Fig. 7 show subtle differences among the models, but Table 1 shows the inner dipole model having the highest average resolution.

Optimized Array

The last test was to create an optimal array comprising 4-pole combinations calculated from the

base 2-pole dataset. The Compare R method was used to calculate 8,000 optimized pairs using the dipole-dipole array as the base set. From Eq. (1), the resistance was calculated for each combination of the optimal array and Fig. 5(d) shows the distribution of resistance data versus geometric factor after filtering to remove obvious outliers. After filtering, using similar criteria as established for the randomly generated array, the final dataset for inverse modeling of the optimized dataset comprised 4,820 values.

Figure 8 shows the resistivity and resolution results for the optimal array. Again, to ensure consistency among the models, the same model grid and inverse model parameters were used to create Fig. 8. The resistivity data show the same low resistivity, high amplitude target at a depth of 20 m as all other models, with slight differences with respect to shape and extent across the profile. For example, the isopleth for a log resistivity value of 1.7 is shown to have separated at a distance of 130 m. The model resolution is shown to be higher than all other arrays, with an average value of 0.14 and the average depth to the 0.063 isopleth at 11.2 m (Table 1). This depth is 3 m below that of the

Rucker and Glaser: Array Conversions from Two-pole Resistance Data

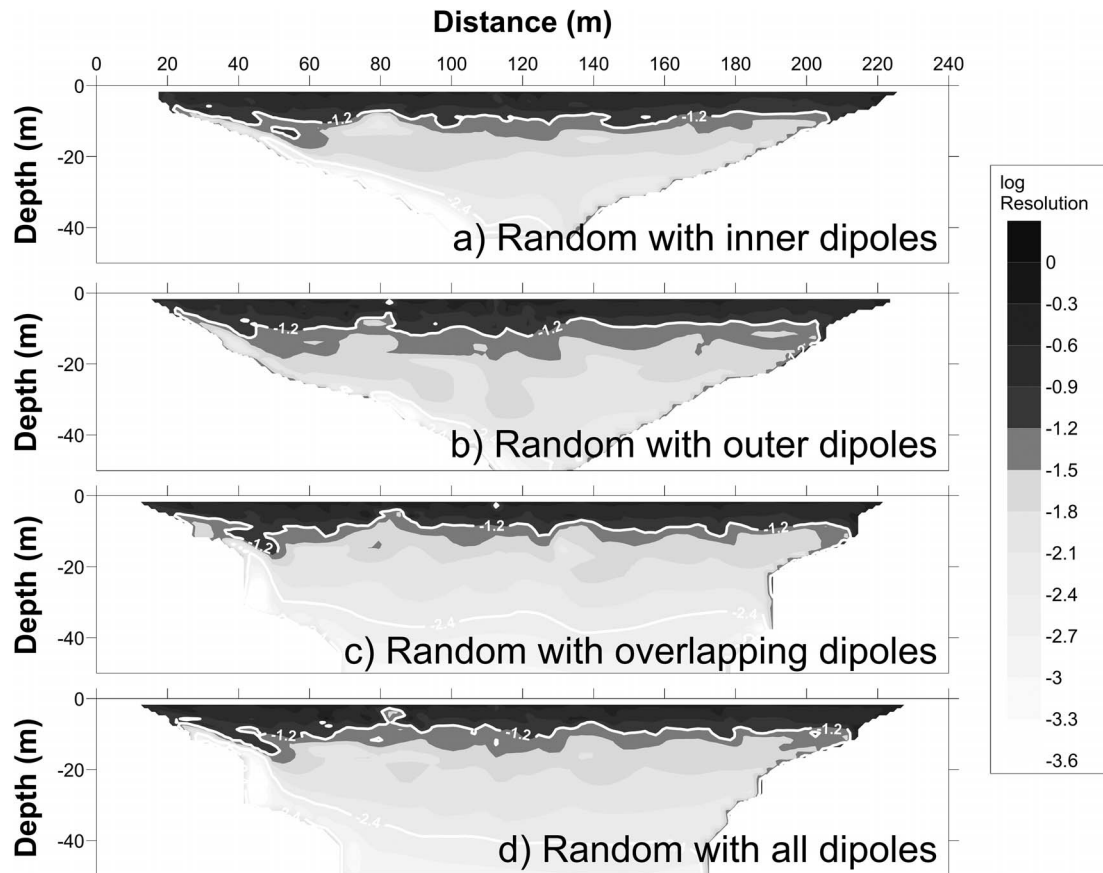


Figure 7. Model resolution from randomly generated dipoles, segregated by a) inner dipoles, b) outer dipoles, c) overlapping dipoles, and d) all dipoles.

dipole-dipole array and shows the power of using an optimized array to resolve pertinent features of the subsurface.

Conclusions

Evaluating different geometric arrays to maximize target recognition is rather popular in electrical resistivity investigations. Often, competing arrays such as the dipole-dipole, Schlumberger, gradient, and other standard configurations are collected simultaneously and modeled together or separately to compare the fidelity of a target's dimensions and resistivity amplitude. To ensure completeness of the study, multiple geological scenarios are usually surveyed and the best array is chosen based on the particular needs of the geophysicist. In this work, we also investigate multiple arrays to test their ability to recreate a hydrogeological target developed from disposal of sodium nitrate waste into a series of infiltration trenches. However, we take a slightly different approach by comparing non-standard arrays reconstructed (*i.e.*, calculated) from a base set of pole-pole data. The reconstruction linearly combines

a series of four 2-pole arrangements to form any desired 4-pole arrangement.

In the first step, we compared the reconstruction of resistance data from the standard arrays of dipole-dipole and Schlumberger to measured data of the same array. The pole-pole array is known for having a high S/N and the reconstruction using 2-pole data showed to be equivalent to and, in a few cases, superior to the measured array in terms of noise. Inverse models were then generated for each array to understand the resolving capabilities of the different measurements. The dipole-dipole array was shown to have the highest model resolution compared to the Schlumberger and pole-pole arrays based on the statistics from the resolution matrix. As a general observation, it appears that those arrays with the shallowest depth of investigation have higher average model resolution.

In the next set of tests, we generated random 4-pole combinations that comprised approximately a third each of inner dipoles, outer dipoles, and overlapping dipoles. These dipoles are equivalent to the Alpha, Beta, and Gamma arrangements, respectively. The resistance data from each type of dipole were plotted

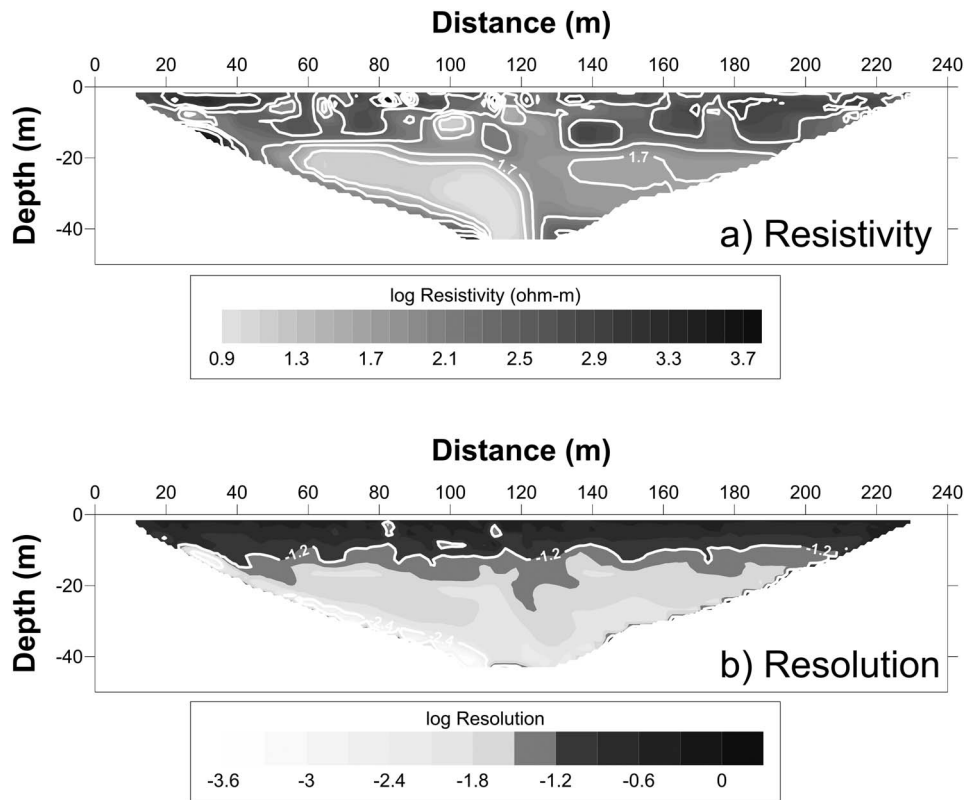


Figure 8. Resistivity and resolution for the optimal array.

against the geometric factor and the inner dipole data were shown to align along a fairly narrow band of apparent resistivity values. The outer and overlapping dipole data had greater amounts of noise with a larger spread in apparent resistivity at larger geometric factors. Inverse models showed that the inner and outer dipoles could reconstruct the nitrate target with similar resistivity attributes as standard arrays, but the model resolution was slightly higher. The higher resolution could be simply from more resistance data being used in the random sets. The models using overlapping dipoles were slightly unstable and the model resolution from them was lower than the dipole-dipole array.

Lastly, a 4-pole optimized array was reconstructed from the 2-pole dataset. The optimization algorithm was based on explicitly increasing the values along the diagonal of the model resolution matrix using the Compare R method. The method searches for combinations that increase the resolution and rejects combinations that decrease the resolution. One constraint of the search criteria was to not consider overlapping dipoles based on their instability in modeling. The reconstructed optimized resistance data were shown to also align along a fairly narrow band of apparent resistivity values. The resistivity inverse model showed a similar target as other arrays, with slightly more detail. The model resolution was shown

to be higher than all other arrays, thus demonstrating that very little effort is needed in acquiring a high quality dataset with low noise and creating a resistivity model with a much better resolvability than what is usually measured. The technique presented herein would seem to be highly advantageous when considering time lapse resistivity monitoring, where low sampling time and high model resolution are competing factors in the survey design (Rucker, 2014).

References

- Al Hagrey, S.A., 2012, 2D optimized electrode arrays for borehole resistivity tomography and CO₂ sequestration modeling: *Pure and Applied Geophysics*, **169**, 1283–1292.
- Batayneh, A.W., 2001, Resistivity imaging for near-surface resistive dyke using two-dimensional DC resistivity techniques: *Journal of Applied Geophysics*, **48**, 25–32.
- Blome, M., Maurer, H., and Greenhalgh, S., 2011, Geoelectric experimental design—Efficient acquisition and exploitation of complete pole-bipole data sets: *Geophysics*, **76**, F15–F26.
- Candansayar, M.E., and Basokur, T., 2001, Detecting small-scale targets by the 2D inversion of two-sided three-electrode data: Application to an archaeological survey: *Geophysical Prospecting*, **49**, 13–25.

Rucker and Glaser: Array Conversions from Two-pole Resistance Data

- Carpenter, E.W., and Habberjam, G.M., 1956, A tri-potential method of resistivity prospecting: *Geophysics*, **21**, 455–469.
- Dahlin, T., and Zhou, B., 2004, A numerical comparison of 2D resistivity imaging with 10 electrode arrays: *Geophysical Prospecting*, **52**, 379–398.
- Dey, A., Meyer, W.H., Morrison, H.F., and Dolan, W.M., 1975, Electrical field response of two-dimensional in homogeneities to unipolar and bipolar electrode configurations: *Geophysics*, **40**, 630–640.
- Gee, G.W., Oostrom, M., Freshley, M.D., Rockhold, M.L., and Zachara, J.M., 2007, Hanford site Vadose Zone studies: An overview: *Vadose Zone Journal*, **6**, 899.
- Gephart, R.E., and Lundgren, R.E., 1995, Hanford tank clean up: A guide to understanding the technical issues: Pacific Northwest National Laboratory, Richland, Washington.
- Kaufmann, O., and Quinif, Y., 2001, An application of cone penetration tests and combined array 2D electrical resistivity tomography to delineate cover-collapse sinkholes prone areas, *in* Geotechnical and environmental applications of karst geology and hydrology, Beck, B.F. and Herring, J.G. (eds.), Balkema, Lisse, 359–364.
- Lehmann, H., 1995, Potential representation by independent configurations on a multi-electrode array: *Geophysical Journal International*, **120**, 331–338.
- Leontarakis, K., and Apostolopoulos, G.V., 2012, Laboratory study of the cross-hole resistivity tomography: The model stacking (MOST) technique: *Journal of Applied Geophysics*, **80**, 67–82.
- Lindenmeier, C.W., Lindberg, M.J., Baum, S.R., Serne, R.J., Clayton, R.E., Geiszler, K.N., Bjornstad, B.N., LeGore, V.L., Valenta, M.M., Lanigan, D.C., Kutnyakov, I.V., and Vickerman, T.S., 2002, Characterization of vadose zone sediment: Borehole C3103 located in the 216-B-7A crib near the B tank farm, PNNL-14128: Pacific Northwest National Laboratory, Richland, Washington.
- Loke, M.H., Chambers, J.E., Rucker, D.F., Kuras, O., and Wilkinson, P.B., 2013, Recent developments in the direct-current geoelectrical imaging method: *Journal of Applied Geophysics*, **95**, 135–156.
- Loke, M.H., Wilkinson, P.B., and Chambers, J.E., 2010a, Fast computation of optimized electrode arrays for 2D resistivity surveys: *Computers & Geosciences*, **36**, 1414–1426.
- Loke, M.H., Wilkinson, P.B., and Chambers, J.E., 2010b, Parallel computation of optimized arrays or 2-D electrical imaging surveys: *Geophysical Journal International*, **183**, 1302–1315.
- Loke, M.H., Wilkinson, P.B., Chambers, J.E., and Strutt, M., 2014, Optimized arrays for 2D cross-borehole electrical tomography surveys: *Geophysical Prospecting*, **62**, 172–189.
- Maurer, H., Boerner, D.E., and Curtis, A., 2000, Design strategies for electromagnetic geophysical surveys: *Inverse Problems*, **16**, 1097–1117.
- Menke, W., 1984, *Geophysical data analysis: Discrete inverse theory*: Academic Press, London.
- Niwas, S., and Israil, M., 1989, Matrix method for the transformation of resistivity sounding data of one electrode configuration to that of another configuration: *Geophysical Prospecting*, **37**, 209–221.
- Rucker, D.F., 2012, Enhanced resolution for long electrode ERT: *Geophysical Journal International*, **191**, 101–111.
- Rucker, D.F., 2014, Investigating motion blur and temporal aliasing from time-lapse electrical resistivity: *Journal of Applied Geophysics*, **111**, 1–13.
- Rucker, D.F., Fink, J.B., and Loke, M.H., 2011, Environmental monitoring of leaks using time lapsed long electrode electrical resistivity: *Journal of Applied Geophysics*, **74**, 242–254.
- Rucker, D.F., Myers, D.A., Cabbage, B.D., Levitt, M.T., Noonan, G.E., McNeill, M., Henderson, C., and Lober, R.W., 2013, Surface geophysical exploration: Developing noninvasive tools to monitor past leaks around Hanford's tank farms: *Environmental Monitoring and Assessment*, **185**, 995–1010.
- Saydam, A.S., and Duckworth, K., 1978, Comparison of some electrode arrays for their IP and apparent resistivity responses over a sheet like target: *Geoexploration*, **16**, 267–289.
- Seaton, W.J., and Burbey, T.J., 2002, Evaluation of two-dimensional resistivity methods in a fractured crystalline-rock terrane: *Journal of Applied Geophysics*, **51**, 21–41.
- Stummer, P., Maurer, H., and Green, A., 2004, Experimental design: Electrical resistivity data sets that provide optimum subsurface information: *Geophysics*, **69**, 120–129.
- Wilkinson, P.B., Loke, M.H., Meldrum, P.I., Chambers, J.E., Kuras, O., Gunn, D.A., and Ogilvy, R.D., 2012, Practical aspects of applied optimized survey design for electrical resistivity tomography: *Geophysical Journal International*, **189**, 428–440.
- Wilkinson, P.B., Meldrum, P.I., Chambers, J.E., Kuras, O., and Ogilvy, R.D., 2006, Improved strategies for the automatic selection of optimized sets of electrical resistivity tomography measurement configurations: *Geophysical Journal International*, **167**, 1119–1126.
- Xu, B., and Noel, M., 1993, On the completeness of data sets with multielectrode systems for electrical resistivity surveys: *Geophysical Prospecting*, **41**, 791–801.
- Zhou, W., Beck, B.F., and Adams, A.L., 2002, Effective electrode array in mapping karst hazards in electrical resistivity tomography: *Environmental Geology*, **42**, 922–928.